energies

MDPI

Article

Measurement and Modeling of Self-Directed Channel (SDC) Memristors: An Extensive Study

Karol Bednarz * and Bartłomiej Garda

Faculty of Electrical Engineering, Automatics, Computer Science and Biomedical Engineering, AGH University of Kraków, al. Mickiewicza 30, 30-059 Kraków, Poland; bgarda@agh.edu.pl
* Correspondence: kbednarz@agh.edu.pl

Abstract: This study systematically addresses the challenge of accurately modeling memristors, focusing on four distinct types doped with tungsten, tin, chromium, and carbon, fabricated by Knowm Inc. A comprehensive characterization is performed by subjecting the devices to sinusoidal excitations with varying frequencies and amplitudes, followed by data averaging and high-frequency filtering. The resulting measurements are fitted using three prominent memristor models: VTEAM, MMS, and Yakopcic. Additional bespoke modifications are assessed. These models, typically formulated as coupled algebraic differential equations integrating electrical quantities (voltage and current) with internal state variables governing device dynamics, are optimized using two robust approaches: (1) interior-point optimization with gradient-based search, and (2) Nelder–Mead gradient-free optimization, both with box constraints applied. A thorough comparison and discussion of the optimized model parameters ensue, accompanied by an examination of the sensitivity to diverse frequency and amplitude ranges. The findings inform conclusions and provide a foundation for future refinements, underscoring the importance of multi-model evaluation and advanced optimization strategies in precise memristor modeling. The presented methodology offers a valuable framework for elucidating optimal modeling paradigms tailored to specific memristor architectures and operating regimes, ultimately enhancing their integration in emerging neuromorphic and computational applications.

Keywords: SDC memristor; memristor modeling; MMS model; VTEAM model; Yakopcic model

Citation: Bednarz, K.; Garda, B. Measurement and Modeling of (SDC) Memristors: An Extensive Study. *Energies* **2024**, *17*, 5400. https://doi.org/10.3390/en17215400

Academic Editors: Ioana-Gabriela Sirbu and Lucian Mandache

Received: 24 August 2024
Revised: 24 October 2024
Accepted: 28 October 2024
Published: 30 October 2024

1. Introduction

Over the past decade, there has been an intense debate surrounding the issue of Moore's Law reaching its limits. This law postulates that the number of transistors in an integrated circuit doubles at nearly regular intervals. With the development of nanometer-scale technology, standard CMOS technology has reached its scalability limits. Consequently, there is a need to find solutions that increase both the performance of modern computers and the amount of available memory. One such idea is to shift from the classic von Neumann architecture, where the processor and memory are separated by a data bus, to an integrated architecture known as in-memory computing. Another idea is to replace the bi-stable transistor with a multistable element. With the emergence of actual memristive devices, both of these ideas seem feasible.

Following Professor Leon Chua's postulation of the memristor in 1971 [1], it took another 37 years for the physical implementation of this element to be achieved. In 2008, the HP Labs team led by R. Stanley Williams published their work on creating a memristor based on titanium dioxide (TiO_2) [2]. Since then, numerous other designs for memristors have emerged, differing in their structure, materials, and operating principles, for example, polymer memristors [3,4], ferroelectric memristors [5], and spintronic memristors [6–8]. One of the most intriguing types of memristors is the Self-Directed Channel (SDC) memristors produced by Knowm Inc., Santa Fe, NM, USA. They have been described in numerous publications [9–11].

Realizing the multitude of memristor designs available today in the design of each prototype circuit, a crucial aspect is simulating the behavior of the circuit under various stimuli. Therefore, it is essential to faithfully replicate the dynamics of memristive elements using their model. This paper will analyze which model best reproduces the behavior of SDC memristors and develop an algorithm to optimize model parameters based on real measurement data. Optimized parameters can be successfully applied in simulation environments such as SPICE or Simulink.

The paper discusses the optimization of parameters for various models based on real measurement data of SDC memristors with different dopings, namely, tungsten, tin, chromium, and carbon, using two algorithms: SQP and Nelder–Mead. Box constraints are imposed on individual parameters during optimization. Since in the paper [12], Strukov, Asymmetric Strukov, and VTEAM models were compared, it is decided to compare other models with the most accurate model from this work, namely the VTEAM model.

The structure of the paper is as follows:

- The "Materials and Methods" section includes a description of the measurement system, signal acquisition methods, and the tools used in the study.
- The "Memristor Models Under Consideration" section provides descriptions of the memristor models that were examined in the text.
- The "Optimization Procedure" section contains a description of the methods and optimization procedures for each of the mathematical memristor models considered.
- The "Optimization Results" section presents the optimization outcomes separately for each of the mathematical memristor models.
- The "Comparative Analysis of Optimization Results" section provides a comparative analysis of memristor models based on the optimization of their parameters.
- The "Conclusion" section presents the key findings derived from the optimization results.

2. Materials and Methods

The SDC (self-directed channel) memristors with tungsten W, carbon C, tin Sn, and chromium Cr doping were subjected to research and measurements.

To measure the current of the memristor and limit it below the nominal value, i.e., 1 mA for memristors doped with W, Sn, Cr and 50 µA for doping with C [10], the memristor was connected in series with a linear resistor R_s. In the case of doping with W, Sn, Cr, the resistance $R_s = 5.11$ [kΩ], while for doping with C, $R_s = 47.5$ [kΩ]. The voltage v_r measured across the resistor R_s, which is a high quality resistor utilized to accurately determine the current of the memristor, according to Ohm's law, is directly proportional to the current and its known resistance, allowing the current of the memristor to be obtained by multiplying the voltage across the resistor by the reciprocal of its resistance. The schematic diagram of the measuring circuit is presented in Figure 1a. Using the myDAQ University Kit device from National Instruments, Austin, TX USA, containing a measurement card and function generator, the supply voltage is generated, and signals v_m and v_z are collected [13]. The current and voltage of the memristor are calculated using Ohm's law and Kirchhoff's second law. The data acquisition and preliminary data processing process is written and implemented in the graphical programming environment *LabVIEW* 2022 [14]. The utilized code is provided in the attached appendices. The circuit connection diagram to the measurement device is shown in Figure 1b.

The voltage across the memristor is calculated using the formula $v_m = v_s - v_r$, and the memristor current is calculated as $i_m = \frac{v_r}{R_s}$.

Before starting measurements, it is necessary for the memristor to be formed. The formation is performed by gradually increasing the voltage to create the necessary conductive paths inside the memristor. However, this voltage should not exceed the nominal operating voltage [10,12]. After forming the memristor, the circuit shown in Figure 1 is powered by a sinusoidal alternating voltage $v_z(t) = V_s \sin(2\pi f t)$ with amplitudes $V_s \in \{0.5, 1, 1.5\}$ [V] and different frequencies, where $f \in \{1, 5, 10, 20, 50, 100\}$ [Hz]. Therefore, 18 tests are

performed for one memristor, where each test consists of 100 periods and 1000 points for each period.

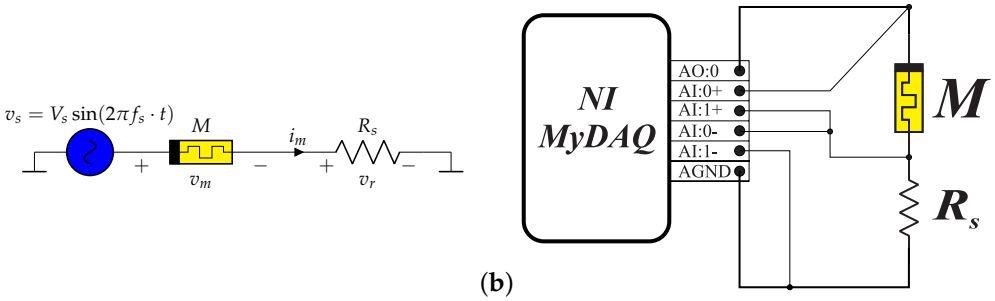

(**a**) (**b**)

Figure 1. The schematics of the measurement setup: (**a**) schematic diagram of the measurement circuit, (**b**) a simplified connection diagram of the measurement device to the circuit.

3. Memristor Models Under Consideration

In the work [12], a comparison is made between the accuracy of various models and actual SDC memristors measurements, focusing on well-known memristor models in the literature, such as the Strukov, Asymmetric Strukov, and VTEAM models. The VTEAM model proves to be the most optimal, while the others demonstrate poor representation of real memristors, likely due to their simplicity. However, this study does not include more advanced models like the MMS model or the Yakopcic model. Therefore, it is decided to compare a slightly modified VTEAM model with these more complex models. Each of the considered models is described in detail in this section.

3.1. MMS Model

To model SDC memristors, a generalized model of metastable memristor proposed by M. Nugent and T. Molter [15] is used. This model is semi-empirical. Each Ag^+ ion cluster is represented as a metastable switch, which probabilistically switches between two states under the influence of voltage and temperature. The switching probability between the HRS (High-Resistance State) and LRS (Low-Resistance State) states is denoted as P_{ON}, while the transition from the LRS to the HRS state is denoted as P_{OFF}. The mathematical dependencies are presented below [15,16]:

$$P_{\mathrm{ON}} = \alpha \frac{1}{1 + e^{-\beta\left(v(t) - V_{\mathrm{ON}}\right)}} \tag{1}$$

$$P_{\mathrm{OFF}} = \alpha \left(1 - \frac{1}{1 + e^{-\beta\left(v(t) + V_{\mathrm{OFF}}\right)}}\right) \tag{2}$$

$$\beta = \frac{q}{kT} \tag{3}$$

where β is the temperature parameter, V_{ON} represents the threshold voltage for the HRS state, V_{OFF} denotes the threshold voltage for the LRS state, q stands for the elementary charge ($1.602176634 \times 10^{-19}$ [C]), k is the Boltzmann constant (1.380649×10^{-23} [J/K]), T represents the absolute temperature in K, $\alpha = \frac{\mathrm{d}t}{\tau}$ is the dimensionless time parameter, and τ represents the time constant in s. The dynamics of the elements is described as the change in the state variable x and is expressed as

$$\frac{\mathrm{d}x}{\mathrm{d}t} = P_{\mathrm{ON}}(1 - x) - P_{\mathrm{OFF}}(x) \tag{4}$$

By combining Equations (1)–(4), we obtain a comprehensive differential equation describing the state variable x as

$$\frac{dx}{dt} = \frac{1}{\tau}\left(\frac{1}{1+e^{-\beta\left(v(t)-V_{ON}\right)}}(1-x) - \left(1-\frac{1}{1+e^{-\beta\left(v(t)+V_{OFF}\right)}}\right)x\right) \tag{5}$$

The variable conductance of the memristor is then the function of the memristor's state and is expressed as [15,16]

$$G_m(x) = \frac{x}{R_{ON}} + \frac{1-x}{R_{OFF}} \tag{6}$$

where R_{ON} is the resistance in the LRS state, and R_{OFF} is the resistance in the HRS state.

3.2. Yakopcic Model

Due to the significant diversity in the types of memristive devices, Yakopcic proposed a new model that introduces multiple parameters, enabling its utilization for accurate circuit simulations and power analyses across a wide range of memristive devices. The relationship between current and voltage depends on the state variable $x(t)$, which governs resistance changes based on physical dynamics. In the described model, the internal variable $x \in \langle 0,1 \rangle$ [17]. The relationship $i(t) = f\Big(x(t), v(t)\Big)$ is presented in Equation (7):

$$i(t) = \begin{cases} a_1 x(t) \sinh\Big(bv(t)\Big), & v(t) \geqslant 0 \\ a_2 x(t) \sinh\Big(bv(t)\Big), & v(t) < 0 \end{cases} \tag{7}$$

where a_1, a_2, b are parameters used for adjustment for various memristive devices:

$$g\Big(v(t)\Big) = \begin{cases} A_p\Big(e^{v(t)} - e^{V_{ON}}\Big), & v(t) > V_{ON} \\ -A_n\Big(e^{-v(t)} - e^{-V_{OFF}}\Big), & v(t) < V_{OFF} \\ 0 & V_{OFF} \leqslant v(t) \leqslant V_{ON} \end{cases} \tag{8}$$

where V_{ON} is the positive threshold voltage, V_{OFF} is the negative threshold voltage, and A_p, A_n are the regulatory quantities of exponential expressions.

The second function $f\Big(x(t)\Big)$ is proposed to model the behavior of the internal variable. It operates based on the assumption that the change of state in the memristive device becomes more difficult at the boundaries of the variable x limitation interval. The algorithm for calculating $f\Big(x(t)\Big)$ is presented below:

If $v(t) > 0$,

$$f\Big(x(t)\Big) = \begin{cases} \omega_p(x, x_{ON})\ e^{-\alpha_p(x-x_{ON})}, & x \geqslant x_{ON} \\ 1, & x < x_{ON} \end{cases}$$

Otherwise,

$$f\Big(x(t)\Big) = \begin{cases} \omega_n(x, x_{OFF})\ e^{\alpha_n(x+x_{OFF}-1)}, & x \leqslant 1 - x_{OFF} \\ 1, & x > 1 - x_{OFF} \end{cases}$$

where x_{ON}, x_{OFF} represent the boundaries of the state variable interval x. Similarly, α_n, α_p characterize the rate of exponent growth, and ω_n, ω_p denote the window functions. Each window function has the following forms:

$$\omega_p(x, x_{ON}) = \frac{x_{ON} - x}{1 - x_{ON}} + 1 \tag{9}$$

$$\omega_n(x, x_{OFF}) = \frac{x}{1 - x_{OFF}} \tag{10}$$

Due to the fact that the modeled state variable should correspond to memristors of various constructions, the equation describing its derivative with respect to time signifi-

cantly differs from the dependence in the Strukov–Williams model (which was introduced to model TiO_2 memristors) and looks as follows [2,17]:

$$\frac{\mathrm{d}x}{\mathrm{d}t} = g\Big(v(t)\Big) f\Big(x(t)\Big) \tag{11}$$

3.3. VTEAM Model

The VTEAM (Voltage Threshold Adaptive Memristor) model is based on the derivative equation of the internal state variable x of the memristor. The VTEAM model combines advantages such as accuracy and generality, but it faces difficulties in optimizing the model due to the parameters that belong to integers. It takes into account the threshold voltages of the memristor at which no change in the state variable occurs. The derivative of the internal variable is expressed by the following relation [12,18]:

$$\frac{\mathrm{d}x}{\mathrm{d}t} = \begin{cases} k_{\mathrm{ON}} \left(\frac{v(t)}{V_{\mathrm{ON}}} - 1 \right)^{\alpha_{\mathrm{ON}}} f_{\mathrm{ON}}(x), & 0 < V_{\mathrm{ON}} \leqslant v \\ 0, & V_{\mathrm{ON}} < 0 < V_{\mathrm{OFF}} \\ k_{\mathrm{OFF}} \left(\frac{v(t)}{V_{\mathrm{OFF}}} - 1 \right)^{\alpha_{\mathrm{OFF}}} f_{\mathrm{OFF}}(x), & v \leqslant V_{\mathrm{OFF}} < 0 \end{cases} \tag{12}$$

where V_{OFF} and V_{ON}, similarly to the previous models described, represent the negative and positive threshold voltages; k_{OFF}, k_{ON} are real parameters where $k_{\mathrm{OFF}} < 0 \wedge k_{\mathrm{ON}} > 0$; α_{OFF}, α_{ON} represent integer parameters; and $f_{\mathrm{ON}}(x)$, $f_{\mathrm{OFF}}(x)$ are window functions. The current–voltage relationship and conductance are not naturally defined by the VTEAM model. A linear current–voltage relationship can be represented by the following formula:

$$i(t) = \left(R_{\mathrm{ON}} + \frac{R_{\mathrm{OFF}} - R_{\mathrm{ON}}}{x_{\mathrm{ON}} - x_{\mathrm{OFF}}} \cdot (x - x_{\mathrm{OFF}}) \right)^{-1} \cdot v(t) \tag{13}$$

where x_{OFF}, x_{ON} represent the range in which the internal state variable x can occur, and R_{ON}, R_{OFF} are the minimum and maximum resistances of the memristor.

4. Optimization Procedure

In this section, the optimization procedure will be described, aimed at finding the optimal parameters for the models described in Section 3.

The discussed optimization involves minimizing a certain objective function F, which is tasked with comparing the waveform of the model function with the actual waveform of the memristor. The requirement is for the function to decrease as the similarity between the resulting model and the estimated actual element waveform increases. The objective function used in this work is a modified coefficient of determination and is defined as [19]

$$F(a,b) = \frac{\mathrm{RSS}(i_m, f(a,b))}{\mathrm{TSS}(i_m)} + \frac{\mathrm{RSS}(v_m, f(a,b))}{\mathrm{TSS}(v_m)} \tag{14}$$

where $f(a,b)$ represents the model function, v_m and i_m denote the memristor voltage and current accordingly, a is the n-th dimension vector of the real valued model parameters ($a \in \mathbb{R}^n$), b is the m-th dimension vector of the integer valued model parameters ($b \in \mathbb{N}^m$), RSS denotes the residual sum of squares, and TSS is the total sum of squares. The functions RSS and TSS take the following form:

$$\mathrm{RSS} = \sum_{i=1}^{n} \Big(y_i - f_i(x) \Big)^2 \tag{15}$$

$$\mathrm{TSS} = \sum_{i=1}^{n} \Big(y_i - \bar{y} \Big)^2 \tag{16}$$

The parameters are as follows: y_i, which represents the actual value of the ith sample; $f_i(x)$ denotes the value predicted by the model; n represents the number of samples in the

period; and $\bar{y}$ is the average value of the samples in the period. The reference values of the memristor current and voltage come from the measured averaged periods of the signal.

During optimization, appropriate values of parameters collected in vectors a and b must be found so that the objective function reaches its minimum. These parameters can be defined as real or natural numbers, depending on the specific model. For parameters that should be natural numbers, the optimization process is performed using the brute-force method, i.e., for each combination within a specified range, and then the ones for which the objective function is the lowest are selected. This algorithm significantly prolongs the optimization time. Parameters that should be natural numbers are the parameters α_{on} and α_{off} in the VTEAM model. Floating-point parameters are also subject to certain constraints, mainly due to the nature of the model. Because the input signal to the system is a continuous sinusoidal function, it is necessary to ensure that the response signal is also a continuous and periodic function. This is ensured when the internal variable of the memristor x is also a continuous and periodic function, so $x(t = 0) = x(t = T)$, where T is the period, indicating that the system is in a steady state. This condition requires optimizing an additional parameter x_{init}, which is a constant of integration when integrating the function of the internal variable and represents the value of the internal variable at the time $t = 0$ of measurement. To ensure the continuity condition, an algorithm is proposed consisting of the preliminary optimization of the objective function described by Equation (14), followed by the optimization of a new objective function, which rewards the continuity and periodicity of the internal variable function as proposed (17):

$$F_{cont}(a, b) = F(a, b) + w\frac{(x_1 - x_{n+1})^2}{x_1^2} \tag{17}$$

Parameters w, x_1, and x_{n+1} are elements of the optimization algorithm. The parameter w is a weight chosen according to the continuity of the function. The parameters x_1 and x_{n+1} are, respectively, the first and last elements of the internal variable function. If condition $|x_1 - x_{n+1}| \leqslant 10^{-3}$ is met, the algorithm terminates its operation; otherwise, the optimization process of function (17) is repeated for $w = w + 1$ until the condition is satisfied. To increase the number of reference points and reduce the integration step, the interpolation method called Akima Spline [20] is utilized, which performs local fitting of the function, and the number of points is increased tenfold. The optimization process for the mentioned models differs slightly. It should be noted that the obtained minima of the objective function may be only the local minima, and there may be parameters for which the objective function can be even lower. The optimization methods are listed in the subsequent subsections.

4.1. MMS Model

Optimization is performed based on six degrees of freedom represented by only the parameters of real value: V_{ON}, V_{OFF}, τ, R_{ON}, R_{OFF}, and x_{init}. Two algorithms are utilized in the optimization process. The first is the *SQP* algorithm implemented in the `fmincon` function of Matlab R2024a [21–23]. The *SQP* method solves a sequence of sub-problems optimizing the quadratic objective model subject to linearized constraints. It ensures box constraints in all iterations and is resilient to objective function results such as `Nan` and `Inf`. It has many advantages, including low memory consumption and the ability to quickly solve problems. However, the solution may be inaccurate due to the barrier function maintaining parameters away from box constraints [22,23] and when the algorithm stacks in the local minima. The second algorithm is the *Nelder–Mead* algorithm, also known as the simplex downhill method. This algorithm does not use the gradient of the objective function [24,25]. It is implemented in the `fminsearch` function of MATLAB; however, the optimization process utilizes the `minimize` function, which is available in the external repository of MATLAB [26]. Unlike the `fminsearch` function, it allows for the introduction of box constraints within which parameters can change.

The optimization process involves initially minimizing the objective function (14) using both algorithms, selecting parameters with the lowest value of this function, then minimizing the function (17) using both algorithms, with parameters obtained in the first stage of minimization, and finally selecting parameters for which the objective function value is the smallest, while simultaneously checking whether the internal variable of the function remains continuous and periodic. A simplified block diagram of the optimization algorithm is shown in Figure 2. Box constraints for individual parameters are presented in Table 1.

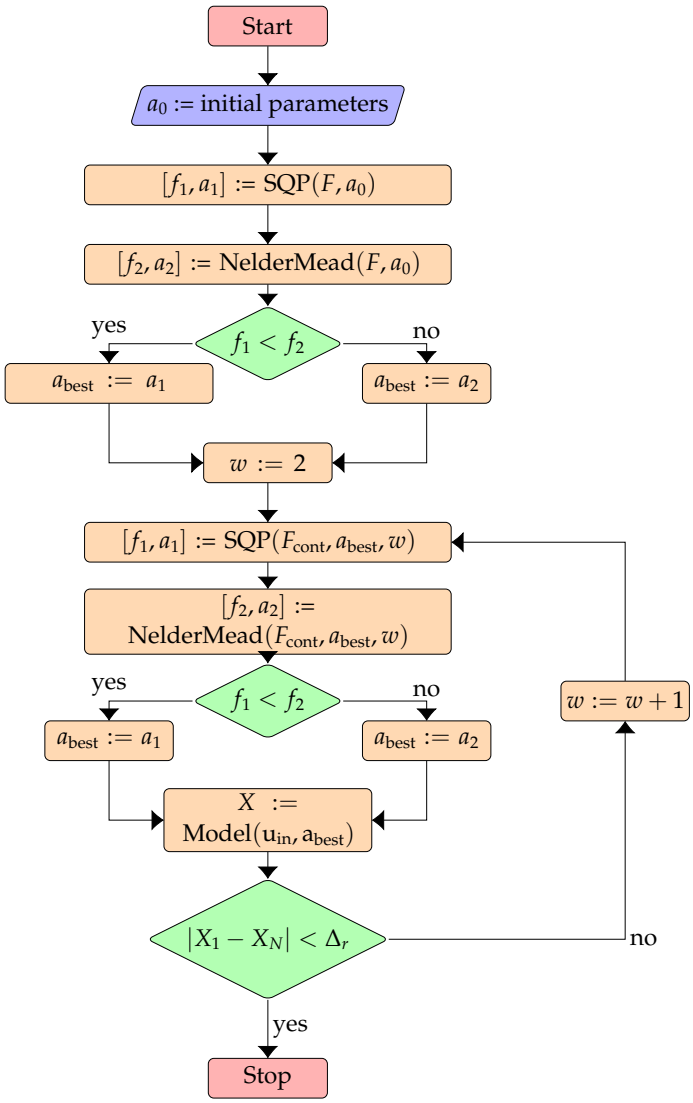

Figure 2. Simplified block diagram of the optimization algorithm.

Table 1. Box constraints on individual parameters during optimization for the MMS model.

Parameter	Range	Parameter	Range
R_{ON}	$0 \div 10$ [kΩ]	R_{OFF}	$0 \div 10$ [MΩ]
V_{ON}	$0 \div 1.5$ [V]	V_{OFF}	$-1.5 \div 0$ [V]
τ	$0 \div 0.1$ [s]	x_{init}	$0 \div 1$

For the simulation and integration of the MMS model, the Runge–Kutta method called "*RK4*" is implemented independently in MATLAB [16,27]. To ensure that the model represents the parameters of a memristor, and not a memristor–linear resistor circuit, the first step is to calculate the value of the internal variable. Subsequently, using the fact that

the relationship $v_m = f(i_m)$ is linear, the memristor conductance can be calculated, as in Equation (6). The voltage is then calculated using a voltage divider $v_m = \frac{v_z}{1+R_s G_m}$, where R_s represents the resistance of the series resistor. Subsequently, the memristor current is the product of the voltage v_m and the conductance G_m.

4.2. VTEAM Model

The optimization is conducted based on nine degrees of freedom, which are v_{ON}, v_{OFF}, k_{ON}, k_{OFF}, R_{ON}, R_{OFF}, α_{OFF}, α_{ON}, and x_{init}. All these parameters are floating-point numbers, except for α_{OFF} and α_{ON}, which should be natural numbers. The optimization process occurs just as for the MMS model described in Section 4.1, except that the optimization process takes place for each combination of the integer pair α_{OFF} and α_{ON}, and then parameters are chosen for the smallest objective function. To limit the dimension of the integer space of the possible solutions, the parameters α_{OFF} and α_{ON} are chosen to be less than 10. Therefore, for a single test, for each amplitude of the driving signal and for each frequency, it is necessary to perform as many as 81 iterations. Additionally, the model employs the Biolek's window function [28] with parameter p: for f_{OFF}, i.e., for the range $v_m \leqslant V_{\mathrm{OFF}} < 0,\ p = 4$, and for f_{ON}, i.e., $0 < V_{\mathrm{ON}} < v_m,\ p = 1$ [18]. In the model, $x_{\mathrm{ON}} = 1$ and $x_{\mathrm{OFF}} = 0$ are set so that the internal variable x can change within a relative range from 0 to 1. The constraints for the optimization parameters are presented in Table 2.

Table 2. Box constraints on individual parameters during optimization for the VTEAM model.

Parameter	Range	Parameter	Range
R_{ON}	$0 \div 10$ [kΩ]	R_{OFF}	$0 \div 1$ [MΩ]
V_{ON}	$0 \div 1.5$ [V]	V_{OFF}	$-1.5 \div 0$ [V]
k_{ON}	$0 \div 5 \times 10^3$	k_{OFF}	$-5 \times 10^3 \div 0$
α_{ON}	$\{1, \ldots, 9\}$	α_{OFF}	$\{1, \ldots, 9\}$
x_{init}	$0 \div 1$		

4.3. Yakopcic Model

The optimization is performed based on twelve degrees of freedom. All the parameters are real. The optimization process is similar to that for the MMS and VTEAM models described in Section 4.1. However, the system is modeled as a "memristor-linear resistor" due to the nonlinear relationship between the memristor current i_m and its voltage v_m as shown in Equation (7). In this equation, it is challenging to directly obtain conductance or resistance since the voltage is an argument of the sinh function. The box constraints for each variable used in the optimization are provided in Table 3.

Table 3. Box constraints on individual parameters during optimization for the Yakopcic model.

Parameter	Range	Parameter	Range
A_p	$0 \div 10^5$	A_n	$0 \div 10^5$
V_{ON}	$0 \div 1$ [V]	V_{OFF}	$-1 \div 0$ [V]
x_{ON}	$0 \div 1$	x_{OFF}	$0 \div 1$
α_p	$0 \div 10^3$	α_n	$0 \div 10^3$
a_1	$0 \div 10^3$	a_2	$0 \div 10^3$
b	$0 \div 10^3$	x_{init}	$0 \div 1$

5. Optimization Results

In this section, the results of the optimization process for each model are presented, discussed, and compared with each other. Due to the high nonlinearity of the objective functions (14) and (17), the calculated minima are likely local, with global minima posing a significant challenge. The optimization process mainly depends on the specified initial points, which must be manually set based on examples from the literature and one's own estimates. In the tests discussed, these are determined experimentally by conducting several optimization trials until a low objective function value is achieved [12].

5.1. MMS Model

Table 4 presents the optimization results. It can be observed that the values of the objective function are quite low, with the majority being lower than 10^{-2}. Figure 3 illustrates a comparison of the current i_m and voltage v_m trajectories of the memristor obtained during measurements with those of the MMS model obtained after optimization, for the lowest value of the objective function. The parameters corresponding to the most favorable case are provided in Table 5. Figure 4a shows the trajectories of the memristor's internal state variable x as a function of the memristor voltage v_m. Meanwhile, Figure 4b presents the trajectory of the internal variable and a comparison of the model's resistance with the measured memristor resistance over time, featuring a logarithmic Y-axis.

Table 4. The objective function values for optimizing the MMS model when supplying the system with sinusoidal voltage of various parameters. The minimum value of the objective function is marked in green, while the maximum is marked in red.

f [Hz]	Tin Doping			Chromium Doping		
	$V_s = 0.5$ V	$V_s = 1$ V	$V_s = 1.5$ V	$V_s = 0.5$ V	$V_s = 1$ V	$V_s = 1.5$ V
1	6.13×10^{-4}	1.32×10^{-3}	1.99×10^{-3}	1.60×10^{-3}	1.09×10^{-2}	1.90×10^{-2}
5	1.41×10^{-3}	2.05×10^{-3}	3.81×10^{-3}	4.03×10^{-3}	1.82×10^{-2}	2.74×10^{-2}
10	6.84×10^{-4}	1.53×10^{-3}	3.77×10^{-3}	5.88×10^{-3}	1.93×10^{-2}	2.12×10^{-2}
20	1.54×10^{-3}	2.04×10^{-3}	1.39×10^{-2}	2.99×10^{-3}	4.64×10^{-2}	1.65×10^{-2}
50	2.16×10^{-3}	2.22×10^{-3}	2.18×10^{-2}	2.62×10^{-3}	9.91×10^{-3}	3.42×10^{-3}
100	9.31×10^{-4}	3.06×10^{-3}	5.74×10^{-3}	8.67×10^{-3}	4.01×10^{-3}	1.28×10^{-2}
f [Hz]	Tungsten Doping			Carbon Doping		
	$V_s = 0.5$ V	$V_s = 1$ V	$V_s = 1.5$ V	$V_s = 0.5$ V	$V_s = 1$ V	$V_s = 1.5$ V
1	2.48×10^{-3}	4.99×10^{-3}	9.93×10^{-3}	1.32×10^{-3}	4.92×10^{-4}	9.12×10^{-4}
5	3.10×10^{-3}	6.23×10^{-3}	1.08×10^{-2}	2.75×10^{-3}	7.36×10^{-4}	7.16×10^{-4}
10	3.64×10^{-3}	5.64×10^{-3}	1.10×10^{-2}	1.38×10^{-3}	7.65×10^{-4}	6.15×10^{-4}
20	3.50×10^{-3}	4.91×10^{-3}	1.04×10^{-2}	1.09×10^{-2}	9.61×10^{-4}	9.95×10^{-4}
50	2.63×10^{-3}	2.27×10^{-3}	1.00×10^{-2}	9.27×10^{-4}	5.43×10^{-3}	1.75×10^{-3}
100	3.01×10^{-3}	8.45×10^{-3}	1.26×10^{-2}	5.08×10^{-2}	1.66×10^{-3}	6.38×10^{-4}

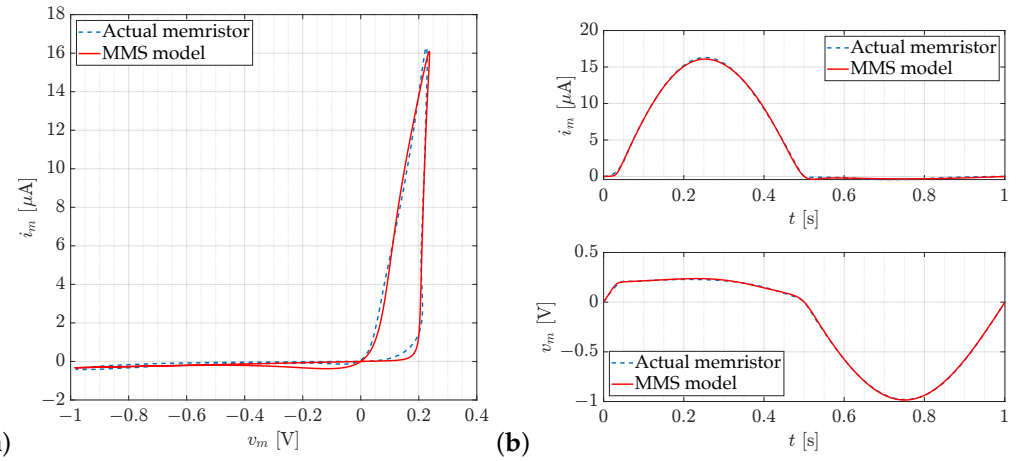

Figure 3. The optimization results obtained for the MMS model with carbon doping, with a supply amplitude of $V_s = 1$ [V] and frequency $f = 1$ [Hz], yield an objective function value for this case of 4.92×10^{-4}. (**a**) Comparison of the hysteresis curves of the memristor $v_m - i_m$, both the reference and the ones obtained during optimization. (**b**) Comparison of the currents and voltages of the memristor with those obtained as a result of model optimization.

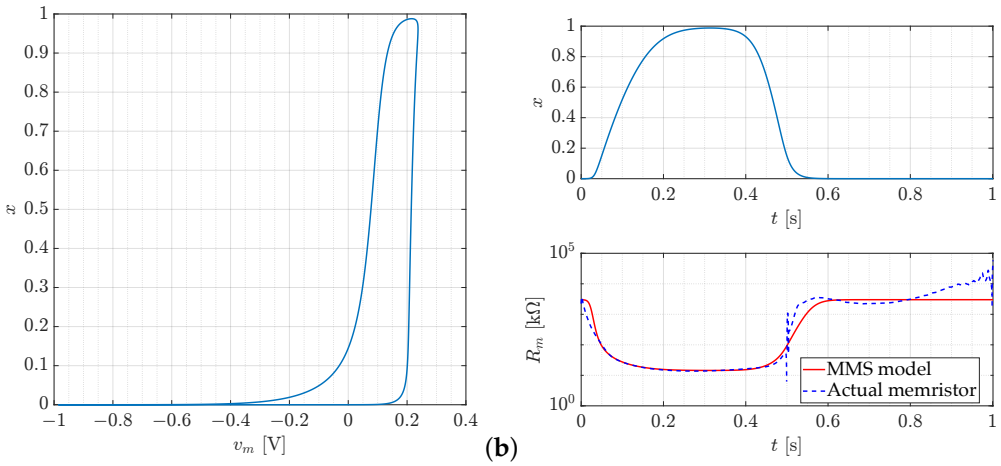

Figure 4. The profiles of the internal variable and resistance obtained for the MMS model with carbon doping, with a supply amplitude of $V_s = 1$ [V] and frequency $f = 1$ [Hz], yield an objective function value for this case of 4.92×10^{-4}. (**a**) The variation in the internal state variable x as a function of the memristor voltage v_m. (**b**) The variation in the internal variable x and the memristor resistance R_m over time.

Table 5. The example of the achieved parameters values for the MMS model for which the lowest objective function value was obtained ($F = 4.92 \times 10^{-4}$). The memristor and excitation signal parameters can be found in the Table 4.

Parameter	Value	Parameter	Value
R_{ON}	14.3 [kΩ]	R_{OFF}	3.02 [MΩ]
V_{ON}	250 [mV]	V_{OFF}	−62.8 [mV]
x_{init}	1.48×10^{-5}	τ	16.8 [ms]

In Table 6, the averaged objective function values over all combinations of the excitation signals for each doping materials are presented. As can be observed, the highest average objective function value is obtained for tungsten doping; however, all these values are close to each other.

Table 6. The averaged objective function values $\bar{F}(a, b)$ for each type of memristor doping after optimizing the MMS model.

Doping	Chromium	Tin	Tungsten	Carbon
$\bar{F}(a, b)$	1.30×10^{-2}	3.92×10^{-3}	6.42×10^{-3}	4.65×10^{-3}

5.2. VTEAM Model

In Table 7, the values of the objective functions are collected. In Figure 5, a comparison of the current i_m and voltage v_m waveforms of the memristor obtained during measurements with the waveforms of the optimized VTEAM model for the minimum value of the objective function is shown. Table 8 provides the parameters corresponding to the most favorable case. In Figure 6a, the variations in the internal state memristor variable x as a function of the memristor voltage v_m are presented. Meanwhile, in Figure 6b, the variation in the internal variable and a comparison of the model resistance with the measured memristor resistance as a function of time are shown. A logarithmic scale is applied to the vertical axis. In Table 9, the averaged objective function values for each doping are presented. As can be observed, the highest average objective function value is obtained for carbon doping, while the lowest is for chromium doping. There is some variation in the values between the memristors doped with chromium and carbon, where the average values differ almost tenfold.

Table 7. The objective function values for optimizing the VTEAM model when supplying the system with sinusoidal voltage of various parameters. The minimum value of the objective function is marked in green, while the maximum is marked in red.

f [Hz]	Tin Doping			Chromium Doping		
	$V_s = 0.5$ V	$V_s = 1$ V	$V_s = 1.5$ V	$V_s = 0.5$ V	$V_s = 1$ V	$V_s = 1.5$ V
1	6.00×10^{-2}	1.16×10^{-3}	8.44×10^{-3}	4.56×10^{-3}	6.92×10^{-4}	4.53×10^{-4}
5	2.19×10^{-3}	2.11×10^{-3}	8.65×10^{-3}	1.14×10^{-2}	1.22×10^{-3}	3.70×10^{-4}
10	3.91×10^{-2}	1.60×10^{-2}	5.60×10^{-3}	3.58×10^{-3}	1.21×10^{-3}	6.72×10^{-4}
20	1.43×10^{-3}	2.64×10^{-2}	1.49×10^{-3}	7.52×10^{-3}	1.32×10^{-3}	9.74×10^{-4}
50	1.25×10^{-3}	3.53×10^{-3}	2.83×10^{-3}	1.19×10^{-2}	4.04×10^{-2}	3.24×10^{-3}
100	1.09×10^{-3}	6.60×10^{-3}	1.93×10^{-2}	6.61×10^{-3}	7.72×10^{-3}	4.92×10^{-4}
f [Hz]	Tungsten Doping			Carbon Doping		
	$V_s = 0.5$ V	$V_s = 1$ V	$V_s = 1.5$ V	$V_s = 0.5$ V	$V_s = 1$ V	$V_s = 1.5$ V
1	2.39×10^{-3}	4.89×10^{-3}	7.77×10^{-2}	5.27×10^{-3}	1.21×10^{-2}	8.48×10^{-3}
5	2.17×10^{-3}	9.81×10^{-2}	8.15×10^{-2}	1.04×10^{-2}	6.69×10^{-3}	2.36×10^{-2}
10	2.43×10^{-3}	4.99×10^{-3}	9.01×10^{-3}	3.76×10^{-2}	0.60	4.24×10^{-3}
20	2.51×10^{-3}	5.20×10^{-3}	6.24×10^{-2}	3.08×10^{-2}	5.72×10^{-3}	1.16×10^{-2}
50	2.24×10^{-3}	0.14	5.51×10^{-2}	5.20×10^{-2}	3.80×10^{-3}	1.21×10^{-2}
100	3.68×10^{-3}	6.57×10^{-3}	8.87×10^{-3}	5.19×10^{-2}	3.35×10^{-3}	2.23×10^{-3}

Table 8. The achieved parameters values of the VTEAM model for which the lowest objective function value is obtained ($F = 3.70 \times 10^{-4}$).

Parameter	Value	Parameter	Value
R_{ON}	620 [Ω]	R_{OFF}	12.6 [MΩ]
V_{ON}	93.4 [mV]	V_{OFF}	−31.7 [mV]
k_{ON}	8.93×10^2	k_{OFF}	-2.71×10^{-3}
α_{ON}	6	α_{OFF}	2
x_{init}	0.81		

Table 9. The averaged objective function values $\bar{F}(a, b)$ for each type of memristor doping after optimizing the VTEAM model.

Doping	Chromium	Tin	Tungsten	Carbon
$\bar{F}(a, b)$	5.79×10^{-3}	1.15×10^{-2}	3.14×10^{-2}	4.88×10^{-2}

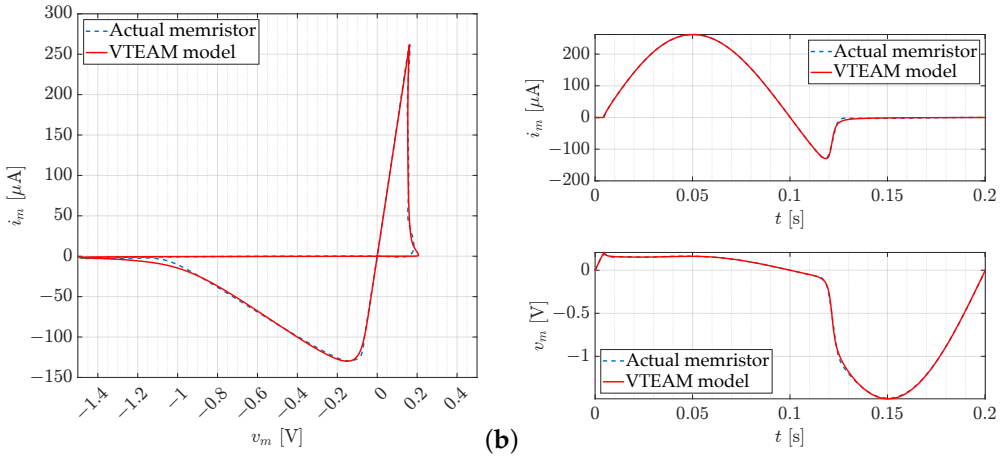

Figure 5. The optimization results obtained for the VTEAM model with chromium doping, with a supply amplitude of $V_s = 1.5$ V and frequency $f = 5$ Hz, yield an objective function value for this case of 3.70×10^{-4}. (**a**) Comparison of the hysteresis curves of the memristor $v_m - i_m$, both the reference and the ones obtained during optimization. (**b**) Comparison of the currents and voltages of the memristor with those obtained as a result of model optimization.

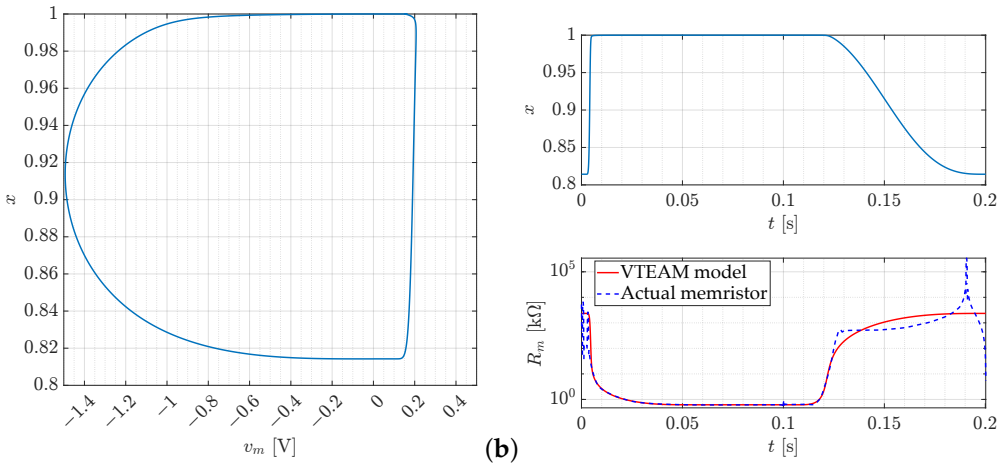

Figure 6. The optimization results obtained for the VTEAM model with chromium doping, with a supply amplitude of $V_s = 1.5\,\text{V}$ and frequency $f = 5\,\text{Hz}$, yield an objective function value for this case of 3.70×10^{-4}. (**a**) The variation in the internal state variable x as a function of the memristor voltage v_m. (**b**) The variation in the internal variable x and the memristor resistance R_m over time.

5.3. Yakopcic Model

As can be observed in Table 10, the objective function values are quite low, with the majority of them being lower than 10^{-2}. In Figure 7, a comparison of the current i_m and voltage v_m waveforms of the memristor obtained during measurements with the waveforms of the Yakopcic model obtained after optimization for the minimum value of the objective function is shown. Table 11 provides the parameters corresponding to the most favorable case. Figure 8a presents the variations in the internal memristor variable x as a function of the memristor voltage v_m, while Figure 8b shows the variation in the internal variable and the memristor resistance as a function of time.

Table 10. The objective function values for optimizing the Yakopcic model when supplying the system with sinusoidal voltage of various parameters. The minimum value of the objective function is marked in green, while the maximum is marked in red.

f [Hz]	Tin Doping			Chromium Doping		
	$V_s = 0.5$ V	$V_s = 1$ V	$V_s = 1.5$ V	$V_s = 0.5$ V	$V_s = 1$ V	$V_s = 1.5$ V
1	4.36×10^{-4}	5.33×10^{-3}	2.21×10^{-3}	7.66×10^{-3}	3.25×10^{-3}	4.35×10^{-3}
5	9.62×10^{-3}	1.04×10^{-2}	1.29×10^{-3}	8.11×10^{-3}	1.19×10^{-2}	5.53×10^{-3}
10	4.33×10^{-3}	1.72×10^{-3}	9.67×10^{-4}	1.04×10^{-2}	7.60×10^{-3}	4.38×10^{-3}
20	5.58×10^{-3}	4.00×10^{-3}	9.49×10^{-3}	6.71×10^{-3}	3.50×10^{-3}	6.44×10^{-3}
50	6.61×10^{-3}	2.86×10^{-3}	1.20×10^{-3}	8.75×10^{-3}	1.23×10^{-2}	8.46×10^{-3}
100	8.87×10^{-3}	4.00×10^{-3}	2.22×10^{-3}	7.15×10^{-3}	5.09×10^{-3}	8.14×10^{-3}
f [Hz]	Tungsten Doping			Carbon Doping		
	$V_s = 0.5$ V	$V_s = 1$ V	$V_s = 1.5$ V	$V_s = 0.5$ V	$V_s = 1$ V	$V_s = 1.5$ V
1	1.75×10^{-3}	5.05×10^{-3}	9.34×10^{-3}	2.00×10^{-3}	3.60×10^{-4}	2.69×10^{-3}
5	1.71×10^{-3}	3.89×10^{-3}	7.91×10^{-3}	2.52×10^{-3}	3.42×10^{-3}	5.57×10^{-3}
10	1.86×10^{-3}	4.15×10^{-3}	8.11×10^{-3}	7.55×10^{-4}	1.52×10^{-3}	1.66×10^{-3}
20	6.56×10^{-3}	3.88×10^{-3}	8.06×10^{-3}	2.40×10^{-2}	1.93×10^{-3}	1.99×10^{-3}
50	2.27×10^{-2}	2.35×10^{-2}	9.41×10^{-3}	3.59×10^{-3}	1.70×10^{-3}	3.40×10^{-3}
100	4.35×10^{-3}	5.77×10^{-3}	9.12×10^{-3}	7.84×10^{-3}	3.54×10^{-3}	1.03×10^{-2}

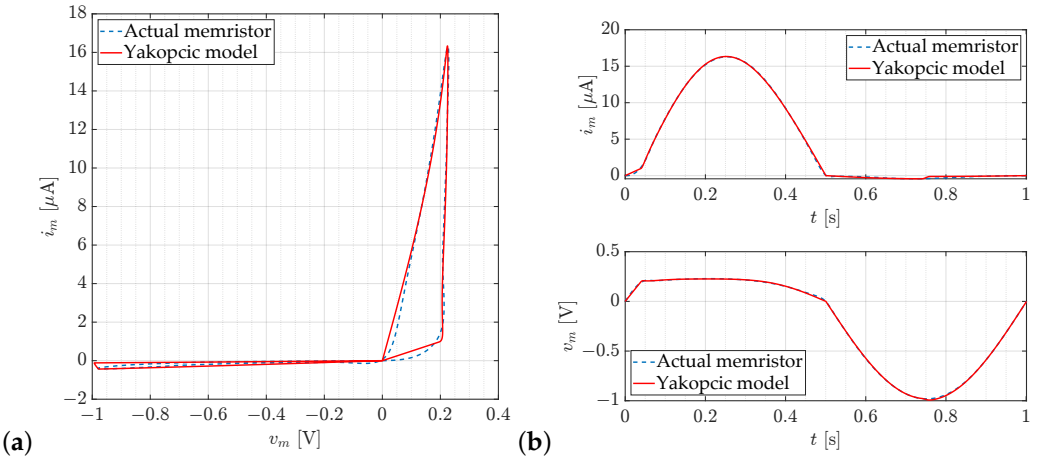

Figure 7. The optimization results obtained for the Yakopcic model with carbon doping, at a supply amplitude of $V_s = 1$ [V] and frequency $f = 1$ [Hz], yield an objective function value of 3.60×10^{-4} for this particular case. (**a**) Comparison of the hysteresis curves of the memristor $v_m - i_m$, both the reference and the ones obtained during optimization. (**b**) Comparison of the currents and voltages of the memristor with those obtained as a result of model optimization.

Table 11. The parameters obtained for the Yakopcic model for the lowest objective function value ($F = 3.60 \times 10^{-4}$).

Parameter	Value	Parameter	Value
A_p	4×10^3	A_n	4×10^3
V_{ON}	243 [mV]	V_{OFF}	-1 [V]
x_{ON}	2.20×10^{-2}	x_{OFF}	0.67
α_p	5.48	α_n	8.01
a_1	2.27×10^{-2}	a_2	7.03×10^{-4}
b	0.67	x_{init}	0.263

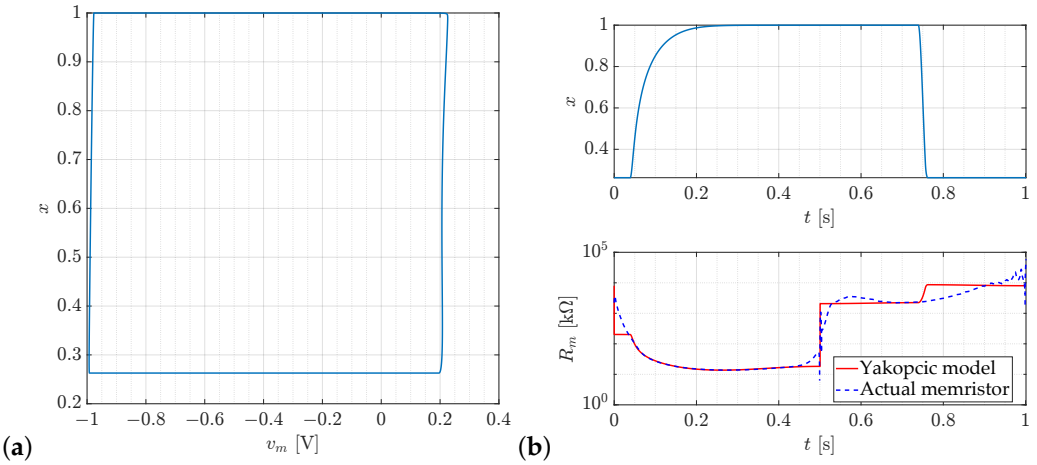

Figure 8. The trajectories of the internal state variable and resistance obtained for the Yakopcic model with carbon doping, at a supply amplitude of $V_s = 1$ [V] and frequency $f = 1$ [Hz], yield an objective function value of 3.60×10^{-4} for this particular case. (**a**) The variation in the internal state variable x as a function of the memristor voltage v_m. (**b**) The variation in the internal variable x and the memristor resistance R_m over time.

In Table 12, the averaged objective function values for each doping are presented. The average objective function values do not significantly differ from each other and are lower than 10^{-2}.

Table 12. The averaged objective function values $\bar{F}(a,b)$ for each type of memristor doping after optimizing the Yakopcic model.

Doping	Chromium	Tin	Tungsten	Carbon
$\bar{F}(a,b)$	7.21×10^{-3}	4.51×10^{-3}	7.62×10^{-3}	4.38×10^{-3}

6. Comparative Analysis of Optimization Results

6.1. Statistical Analysis of the Optimization Results Obtained

To facilitate a comparative analysis of the optimized models, several comparative graphs have been generated. Figure 9 illustrates the average objective function values for each model as a function of the supply voltage amplitude applied to the memristor–resistor system. It is readily apparent that the VTEAM model exhibits the highest objective function values, accompanied by a significant dispersion as indicated by the error bars associated with each data point. The error bars represent confidence intervals, which are intrinsically linked to the probability distribution of the measured values [29]. Notably, the MMS and Yakopcic models demonstrate a reduced dispersion of the results. The objective function value for the MMS model increases with increasing the supply signal, in contrast to the Yakopcic model.

Figure 10 depicts the average objective function values for each model as a function of the frequency of the supply voltage applied to the memristor–resistor system. It is immediately evident that the VTEAM model exhibits the highest objective function values, accompanied by a significant dispersion, as indicated by the error bars. In contrast, the MMS and Yakopcic models demonstrate a reduced dispersion of the results and considerably lower average objective function values. In particular, the Yakopcic and MMS models exhibit lower objective function values within the lower frequency range.

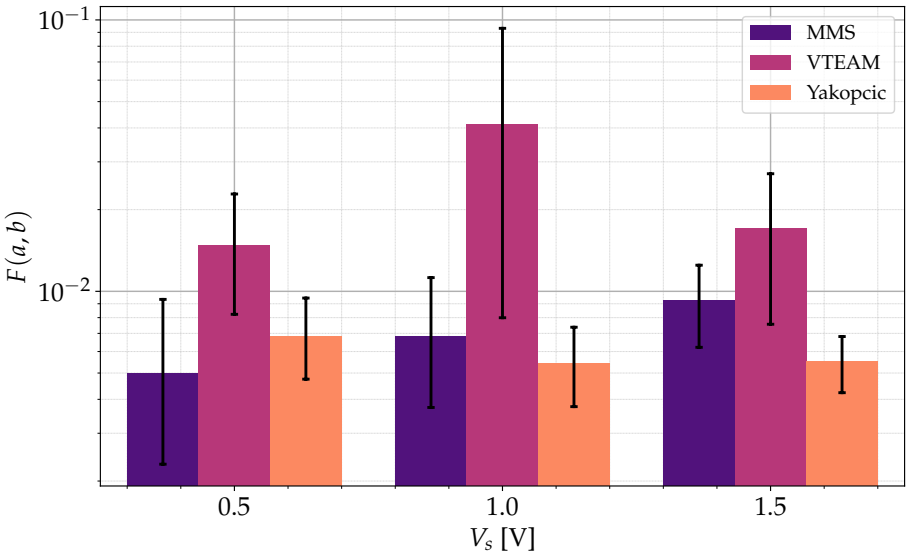

Figure 9. The average objective function values for each model as a function of the supply voltage amplitude applied to the memristor–resistor system. The *y*-axis is presented on a logarithmic scale.

Figure 11 presents the average values of the objective function for each model as a function of the doping material used. It is evident that for the MMS model, the lowest average objective function values are observed for tin and carbon doping, while the highest value corresponds to chromium doping. Similarly, the Yakopcic model exhibits the lowest objective function values for carbon and tin doping, with the highest value associated with tungsten doping. In the VTEAM model, the highest values are obtained for carbon doping and the lowest values are obtained for chromium doping.

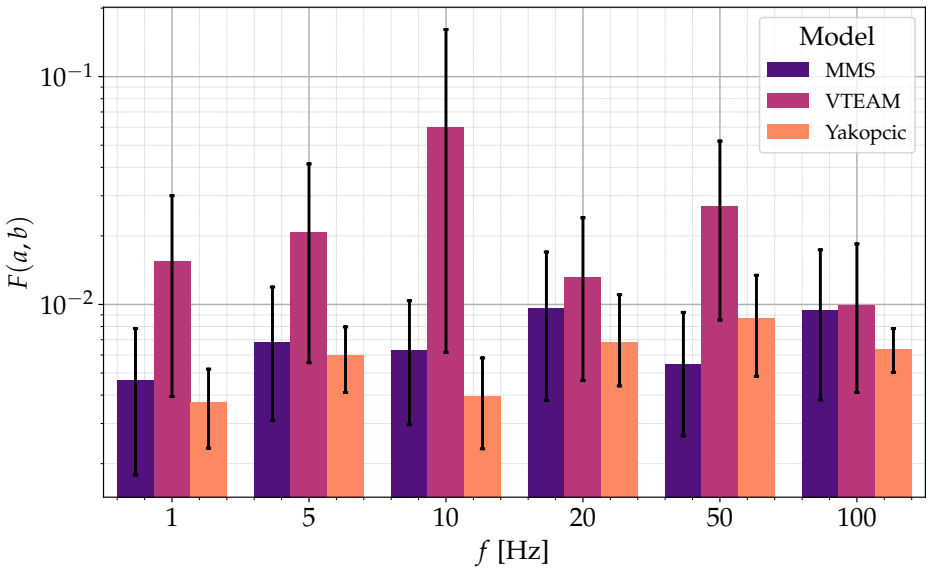

Figure 10. The average objective function values for each model as a function of the frequency of the supply voltage applied to the memristor–resistor system. The y-axis is presented on a logarithmic scale.

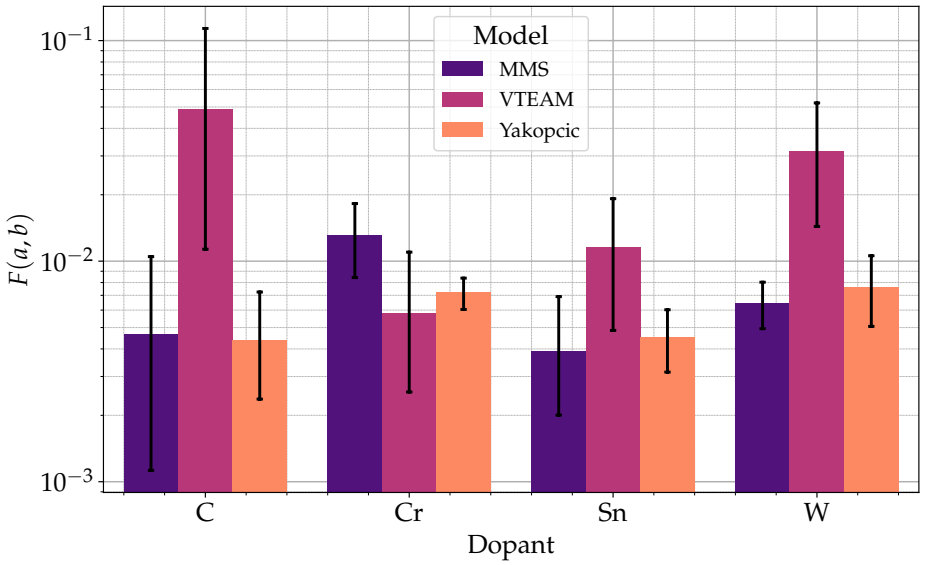

Figure 11. The average objective function values for each model as a function of the memristor doping material. The y-axis is presented on a logarithmic scale.

Figure 12 presents a box plot [30] that illustrates the distribution of the obtained objective function values. It is evident that the median objective function value is lowest for the MMS model and highest for the VTEAM model. Furthermore, the VTEAM model exhibits the greatest dispersion of values. The value axis of the objective function is presented on a logarithmic scale to enhance data clarity.

Table 13 displays the average objective function values for each model. The Yakopcic model exhibits the lowest average objective function value, which is marginally lower than that of the MMS model, at 5.93×10^{-3}. The VTEAM model presents the highest objective function value. Table 14 presents the standard deviation (σ) of the objective function values for each model. Notably, the Yakopcic model demonstrates the lowest standard deviation at 4.79×10^{-3}, while the VTEAM model exhibits the highest at 7.30×10^{-2}.

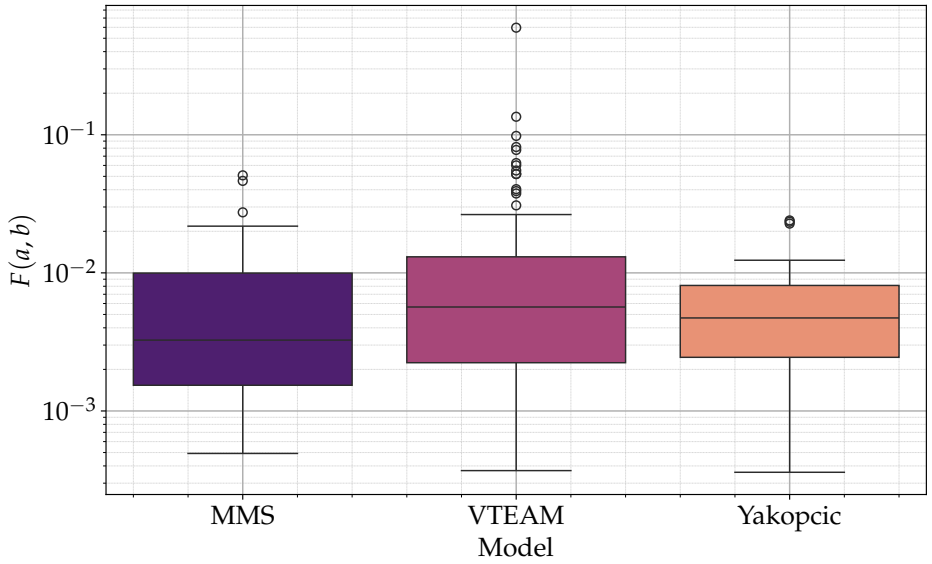

Figure 12. Box plot of the objective function values for each model.

Table 13. Mean values of the objective function for each of the models. The highest objective function is marked in red, while the lowest is marked in green.

Model	MMS	VTEAM	Yakopcic
$\bar{F}(a,b)$	7.01×10^{-3}	2.44×10^{-2}	5.93×10^{-3}

Table 14. Mean values of the objective function for each of the models. The highest objective function is indicated in red, and the lowest in green.

Model	MMS	VTEAM	Yakopcic
σ	9.33×10^{-3}	7.30×10^{-2}	4.79×10^{-3}

6.2. Analysis of Results in the Context of Parameter Generalization

A critical factor essential for the simulation of electric circuits is that the parameters of the models remain invariant with respect to changes in the operational conditions under which these models function, such as the form of the excitation, its amplitude, and frequency. In this subsection, the examination how the optimal parameters of models, determined through optimization, vary with the frequency and amplitude of the input signal is presented. Additionally, the exploration of how the optimal parameters for different types of excitation influence the objective function's value for other excitation parameters is carried out.

In Figure 13, an exemplary heatmap is presented, displaying the objective function values for the evaluation of model parameters obtained through optimization for different excitation parameters. As can be observed, the lowest values of the objective function are located along the diagonal of the matrix. This is because these are the objective function values for the parameters for which the optimization is performed. The values in the upper right corners of the matrix are the highest. These are the regions where the objective function values are evaluated for the most divergent excitation parameters from those used during the optimization process. From the presented graph, it can be concluded that the parameters of the MMS models do not generalize the dynamics of memristors for all operational conditions. An interesting aspect is the significantly higher accuracy of the model when it is optimized at higher excitation frequencies and evaluated at lower frequencies, rather than the other way around.

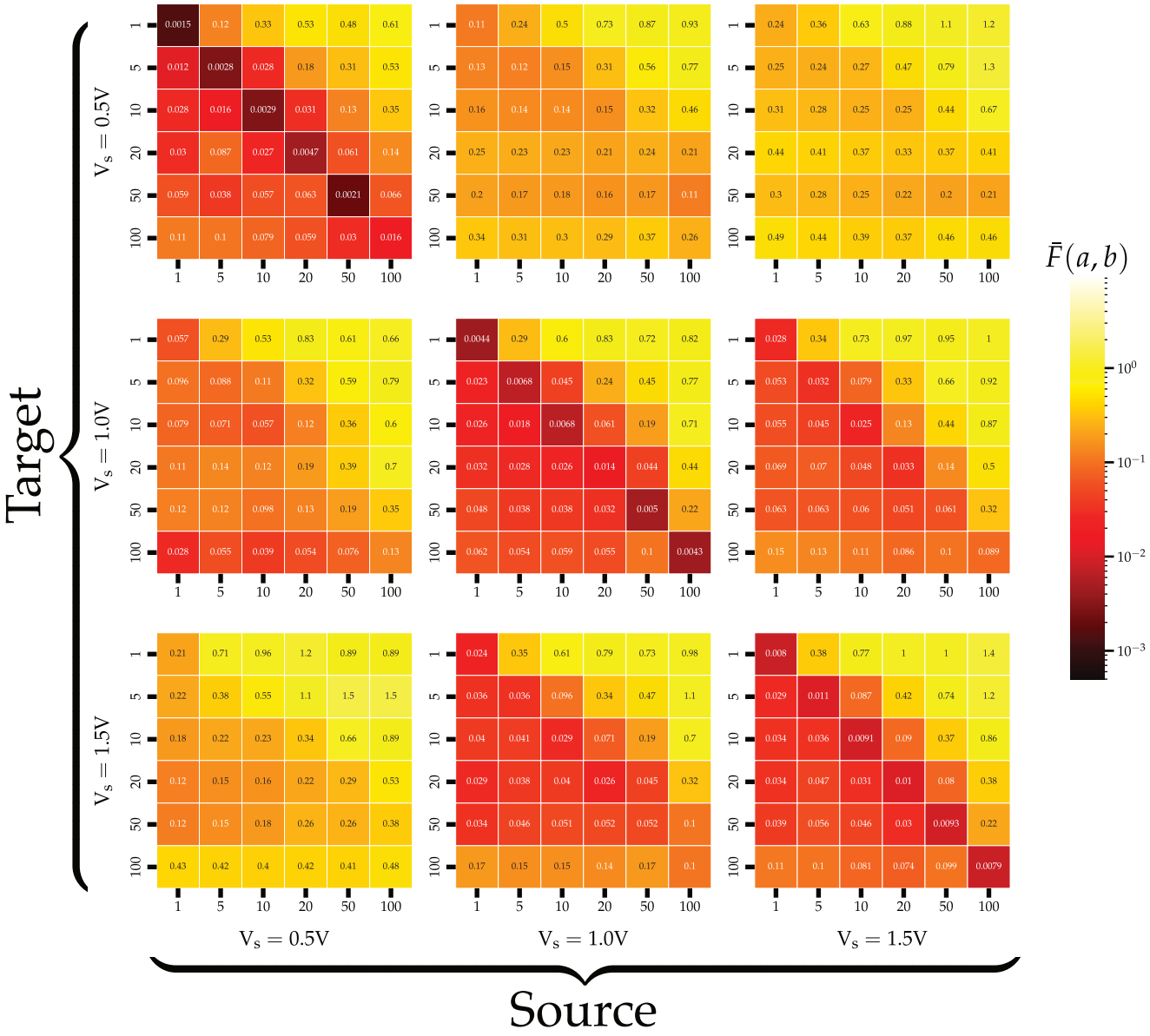

Figure 13. An exemplary matrix in the form of a heatmap, where both color and annotation depict the value of the averaged objective function, is presented. On the left side of the graph are the excitation parameters for which the model is optimized, while along the bottom are the excitation parameters for which the model is evaluated. The graph contains data from the MMS model. For enhanced visibility, the color scale is logarithmically adjusted.

In Figure 14, a matrix of plots is presented, showing the variation in MMS model parameter values (Y-axis) with linear trend lines, depending on the doping of the memristors and excitation parameters (X-axis). As can be observed, the optimized parameters of the MMS model change quite drastically depending on the excitation signal parameters (in this case, the parameters of the alternating supply voltage). This requires adjusting the model parameters during simulation according to the intended signal.

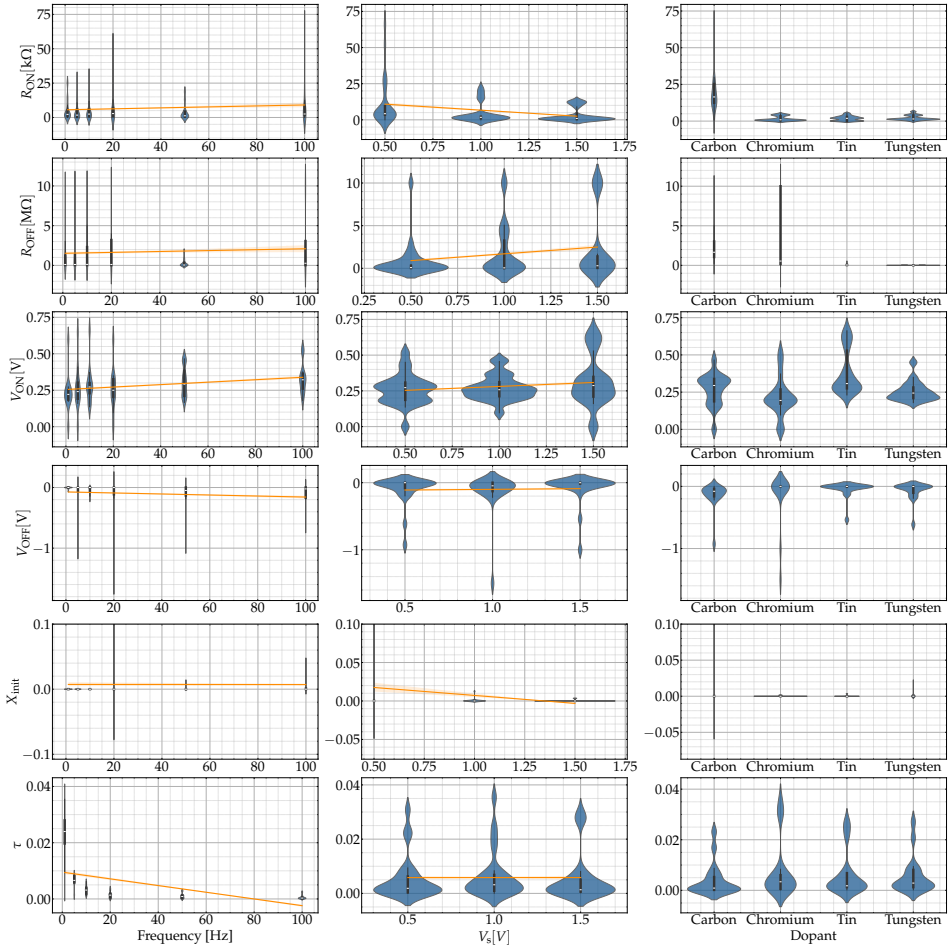

Figure 14. A matrix of plots illustrating the variation in MMS model parameter values (y-axis) with linear trend lines, depending on the doping of memristors and excitation parameters (x-axis), is presented.

7. Conclusions

From the conducted optimizations, it can be concluded that they were successful, and the obtained objective functions achieved relatively low values. It can also be inferred that the best models for modeling SDC memristors are the MMS and Yakopcic models. They have similar low average values of the objective function, and the dispersion of these values is not large depending on the amplitude of the supply voltage, frequency, or type of doping. Compared to the models mentioned earlier, the worst model for optimization is definitely the VTEAM model. It has the highest average values of the objective function and the largest dispersion. Taking into account the specifics of the model, especially the fact that natural parameters are required, the optimization of this model is quite tedious due to iterating over all possible combinations of integer parameters in the interval and selecting the best solution. This means that the time needed to minimize the objective function is several dozen times longer than the time needed for the MMS model. An additional problem is the undefined values by the objective function, which the minimizing algorithm must be resistant to. Taking into account also the specifics of individual models, it can be reflected that the MMS model is best suited for modeling SDC memristors due to its simplicity (only six degrees of freedom), the linear dependence of the current on the voltage, and the fact that it does not have threshold ranges, so the function of the internal variable is monotonically continuous. The MMS model also has a physical interpretation in real memristors. The Yakopcic model was created to fit every type of memristor, and in the discussed case, quite good fits and low objective functions are obtained. However, it is

quite complicated and does not have a linear dependence of the current on the voltage. Additionally, it is a mathematical concept and does not have a physical interpretation.

From the optimization results, it can also be concluded that the lowest objective functions are obtained for fairly rounded waveforms where there is no sudden switching between states, which is called soft switching [16]. It occurs when the function of the internal variable x does not reach the upper value of the range in which it is contained. This is especially visible when powered by signals with high frequency and low amplitude, as the energy and charge in each half-period are low and do not allow reaching the limit ranges of the internal variable. During the measurements, the influence of the memristor temperature change has been observed. In the future, the authors will consider participation in the project of creating the optimal memristor model with temperature as the additional parameter involved. The first idea seems to extend the MMS memristor model of this additional feature.

In summary, the most significant conclusions drawn from this study are as follows:

- The automatic and precise selection of the parameters of the memristor model is achieved successfully, eliminating the need for manual estimation, which typically leads to reduced accuracy.
- This achievement enables faster prototyping of circuits incorporating memristors, thanks to the high correspondence between the models and the experimental data.
- The MMS model, specifically designed for this purpose, is identified as the most suitable for modeling SDC memristors. This is due to its simplicity, the absence of discontinuities, and its ease of integration (even with suboptimal parameters, the solutions remain convergent).
- However, further research is needed to generalize the memristor models, ensuring that, once optimized, the parameters accurately represent memristors operating under a variety of conditions.

Author Contributions: Conceptualization, B.G.; methodology, B.G. and K.B.; software, K.B.; validation, K.B. and B.G.; resources, B.G. and K.B.; data curation, K.B.; writing—original draft preparation, K.B. and B.G.; writing—review and editing, K.B. and B.G.; visualization, K.B.; supervision, B.G. All authors have read and agreed to the published version of the manuscript.

Funding: The research presented in the article was financed by (1) the Polish Ministry of Science and Higher Education as part of a subsidy for AGH University of Krakow, (2) Academic grant from Faculty of Electrical Engineering, Automatics, Computer Science and Biomedical Engineering, AGH University of Kraków, Poland.

Data Availability Statement: The data acquired during measurements have been publicly shared on the Kaggle platform at the following link: kaggle.com/datasets/karolbednarz/modelling-memristor-dataset (accessed on 23 August 2024). The programming algorithms can be obtained from GitHub platform at the following link: https://github.com/mancorz98/MemristorModelOptimization/tree/main (accessed on 22 September 2024).

Conflicts of Interest: The authors declare no conflicts of interest.

References

1. Chua, L. Memristor-The missing circuit element. *IEEE Trans. Circuit Theory* **1971**, *18*, 507–519. [CrossRef]
2. Strukov, D.; Snider, G.; Stewart, D.; Williams, S. The Missing Memristor Found. *Nature* **2008**, *453*, 80–83. [CrossRef]
3. Mladenov, V. *Advanced Memristor Modeling*; MDPI: Basel, Switzerland, 2019. [CrossRef]
4. Chen, Y.; Liu, G.; Wang, C.; Zhang, W.; Li, R.W.; Wang, L. Polymer memristor for information storage and neuromorphic applications. *Mater. Horiz.* **2014**, *1*, 489–506. [CrossRef]
5. Hu, Z.; Li, Q.; Li, M.; Wang, Q.; Zhu, Y.; Liu, X.; Zhao, X.; Liu, Y.; Dong, S. Ferroelectric memristor based on Pt/$BiFeO_3$/Nb-doped $SrTiO_3$ heterostructure. *Appl. Phys. Lett.* **2013**, *102*, 102901. [CrossRef]
6. Wang, L.; Yang, C.; Wen, J.; Gai, S.; Peng, Y. Overview of emerging memristor families from resistive memristor to spintronic memristor. *J. Mater. Sci. Mater. Electron.* **2015**, *26*, 4618–4628. [CrossRef]
7. Wang, X.; Chen, Y. Spintronic memristor devices and application. In Proceedings of the 2010 Design, Automation & Test in Europe Conference & Exhibition (DATE 2010), Dresden, Germany, 8–12 March 2010; pp. 667–672. [CrossRef]

8. Nafea, S.F.; Dessouki, A.A.; El-Rabaie, S.; Elnaghi, B.E.; Ismail, Y.; Mostafa, H. An accurate model of domain-wall-based spintronic memristor. *Integration* **2019**, *65*, 149–162. [CrossRef]
9. Garda, B.; Bednarz, K. Comprehensive Study of SDC Memristors for Resistive RAM Applications. *Energies* **2024**, *17*, 467. [CrossRef]
10. Knowm Inc. *Knowm Self Directed Channel Memristors Data Sheet*, Rev. 3.2 ed.; Knowm Inc.: Santa Fe, NM, USA, 2019. Available online: www.knowm.com (accessed on 25 March 2023).
11. Campbell, K.A. Self-directed channel memristor for high temperature operation. *Microelectron. J.* **2017**, *59*, 10–14. [CrossRef]
12. Garda, B. Modeling of Memristors under Periodic Signals of Different Parameters. *Energies* **2021**, *14*, 7264. [CrossRef]
13. National Instruments, 11500 N Mopac Expwy. *User Guide Ni myDAQ*; National Instruments: Austin, TX, USA, 2023.
14. Elliott, C.; Vijayakumar, V.; Zink, W.; Hansen, R. National Instruments LabVIEW: A Programming Environment for Laboratory Automation and Measurement. *J. Assoc. Lab. Autom.* **2007**, *12*, 17–24. [CrossRef]
15. Ostrovskii, V.; Fedoseev, P.; Bobrova, Y.; Butusov, D. Structural and Parametric Identification of Knowm Memristors. *Nanomaterials* **2022**, *12*, 63. [CrossRef] [PubMed]
16. Ma, G.; Man, M.; Zhang, Y.; Liu, S. Electromagnetic Interference Effects of Continuous Waves on Memristors: A Simulation Study. *Sensors* **2022**, *22*, 5785. [CrossRef] [PubMed]
17. Yakopcic, C.; Taha, T.M.; Subramanyam, G.; Pino, R.E.; Rogers, S. A Memristor Device Model. *IEEE Electron Device Lett.* **2011**, *32*, 1436–1438. [CrossRef]
18. Kvatinsky, S.; Ramadan, M.; Friedman, E.G.; Kolodny, A. VTEAM: A General Model for Voltage-Controlled Memristors. *IEEE Trans. Circuits Syst. II Express Briefs* **2015**, *62*, 786–790. [CrossRef]
19. Renaud, O.; Victoria-Feser, M.P. A robust coefficient of determination for regression. *J. Stat. Plan. Inference* **2010**, *140*, 1852–1862. [CrossRef]
20. Akima, H. A new method of interpolation and smooth curve fitting based on local procedures. *J. ACM* **1970**, *17*, 589–602. [CrossRef]
21. Fliege, J.; Vaz, A.I.F. A Method for Constrained Multiobjective Optimization Based on SQP Techniques. *SIAM J. Optim.* **2016**, *26*, 2091–2119. [CrossRef]
22. López, C.P. *MATLAB Optimization Techniques*; Springer Nature: Berlin/Heidelberg, Germany, 2014. [CrossRef]
23. Choosing the Algorithm—MATLAB & Simulink. Available online: https://www.mathworks.com/help/optim/ug/choosing-the-algorithm.html#btr9d6u (accessed on 25 March 2023).
24. Fminsearch Algorithm—MATLAB & Simulink. Available online: https://www.mathworks.com/help/optim/ug/fminsearch-algorithm.html (accessed on 25 March 2023).
25. Luersen, M.A.; Le Riche, R. Globalized Nelder–Mead method for engineering optimization. *Comput. Struct.* **2004**, *82*, 2251–2260. [CrossRef]
26. Oldenhuis, R. FEX-Minimize. Available online: https://github.com/rodyo/FEX-minimize (accessed on 25 March 2023).
27. Burden, R.L.; Faires, J.D. *Numerical Analysis*; Cengage Learning: Boston, MA, USA, 2010.
28. Mladenov, V.; Kirilov, S. A Nonlinear Drift Memristor Model with a Modified Biolek Window Function and Activation Threshold. *Electronics* **2017**, *6*, 77. [CrossRef]
29. Poole, C. Beyond the confidence interval. *Am. J. Public Health* **1987**, *77*, 195–199. [CrossRef]
30. Williamson, D.; Parker, R.; Kendrick, J. The box plot: A simple visual method to interpret data. *Ann. Intern. Med.* **1989**, *110*, 916–921. [CrossRef]